Fusco et al., http://www.jcb.org/cgi/content/full/jcb.201506018/DC1

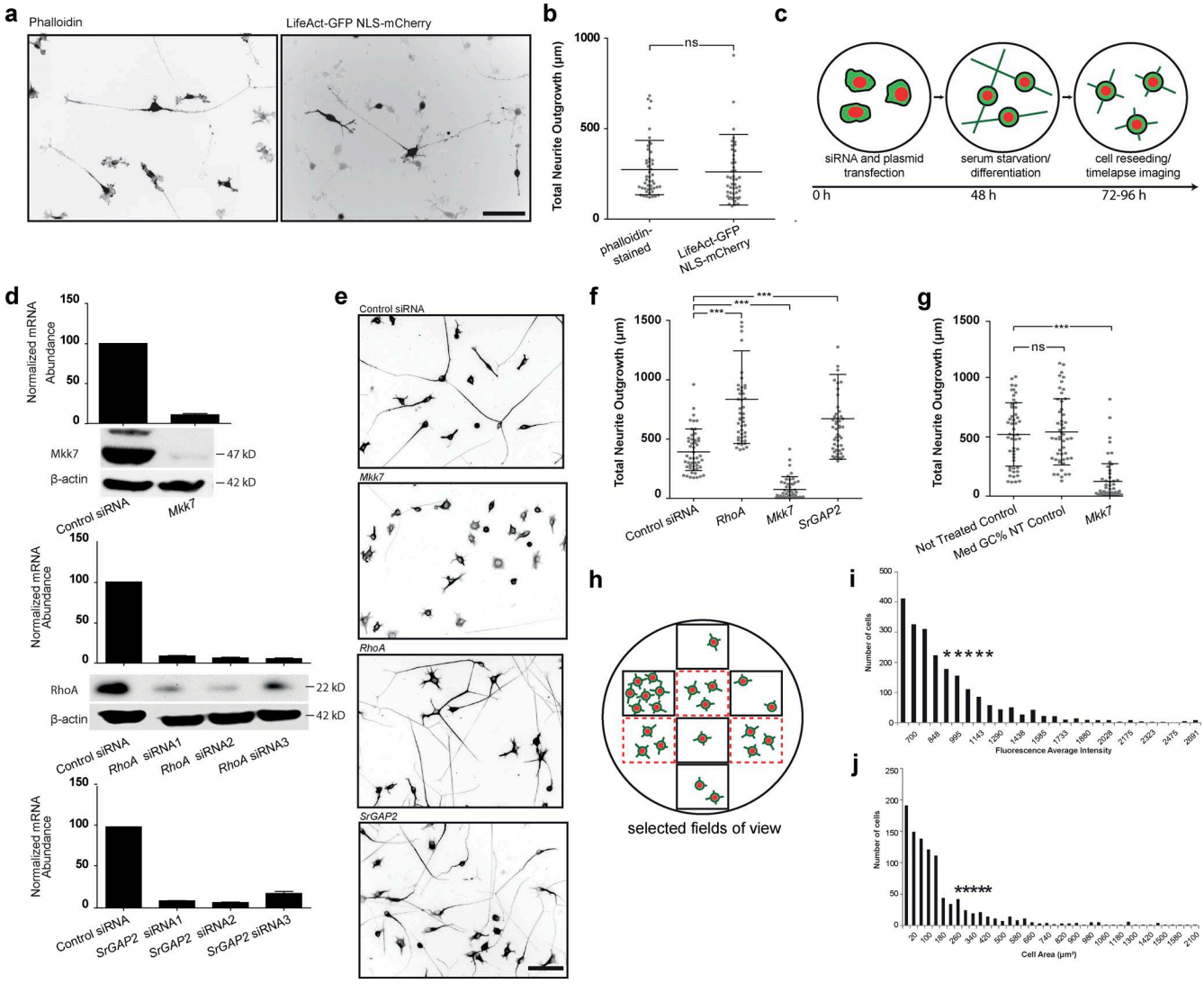

Figure S1. **High-content live-cell imaging platform and RNAi pipeline.** (a) Neurite outgrowth representative images of untransfected, phalloidin-stained versus Lifeact-GFP/NLS-mCherry transfected, unstained cells. Inverted black-and-white contrast is shown. Bar, 100 µm. (b) Total neurite outgrowth quantification of a. Images were segmented and quantified using the Metamorph neurite outgrowth plugin using phalloidin stainings (nontransfected cells) or the Lifeact-GFP signal (reporter-transfected cells). Population mean ± standard deviations are shown for 20% cells with highest total neurite outgrowth (n = 50 cells). t test was used. Ns, nonsignificant. (c) Schematic representation of transfection and cell differentiation during the siRNA screen. In brief, cells are seeded on day 1, transfected with siRNAs or reporter plasmids on day 2, differentiated by serum starvation on day 3, and replated on laminin-coated coverslips on day 4 for 20 h (time-lapse experiments) or 24 h (steady-state neurite outgrowth measurements). (d) Western blot and quantitative PCR quantification of *Mkk7*, *RhoA*, and *SrGAP2* KD efficiencies. Mean ± standard deviations from at least three experiments are shown for quantitative PCR data. (e) Representative images of α-tubulin-stained *Mkk7*, *RhoA*, and *SrGAP2* KD cells. Bar, 100 µm. (f) Total neurite outgrowth quantification of *Mkk7*, *RhoA*, and *SrGAP2* KD experiments. Images were segmented and quantified using the Metamorph neurite outgrowth plugin. (g) Total neurite outgrowth quantifications of nontransfected cells, cells transfected with a nontargeting control siRNA with medium GC content, or *Mkk7* siRNA. (f and g) Population mean ± standard deviation is shown for 20% cells with longest total neurite outgrowth are shown (n = 50 cells). One-way ANOVA with Bonferroni's multiple comparison test was used. ***, $P < 0.0001$. (h) Schematics of field-of-view selection with appropriate cell numbers and fluorescence intensities. 3 h after replating of reporter- or siRNA-transfected cells, a Metamorph macro was used to comprehensively scan multiple fields of view of each well of the 24-well plate. On each field of view, cell somata were then automatically segmented, and their area and mean fluorescence intensity were computed. 10 fields of view with appropriate cell number and fluorescence intensities were then selected (represented by a dashed red outline). (i and j) Fluorescence intensity (i) and cell area (j) criteria used to select appropriate fields of view. Occurrence plots of fluorescence intensity (i) and cell area (j) values are shown. Fields of view containing cells with values denoted by multiple asterisks were selected.

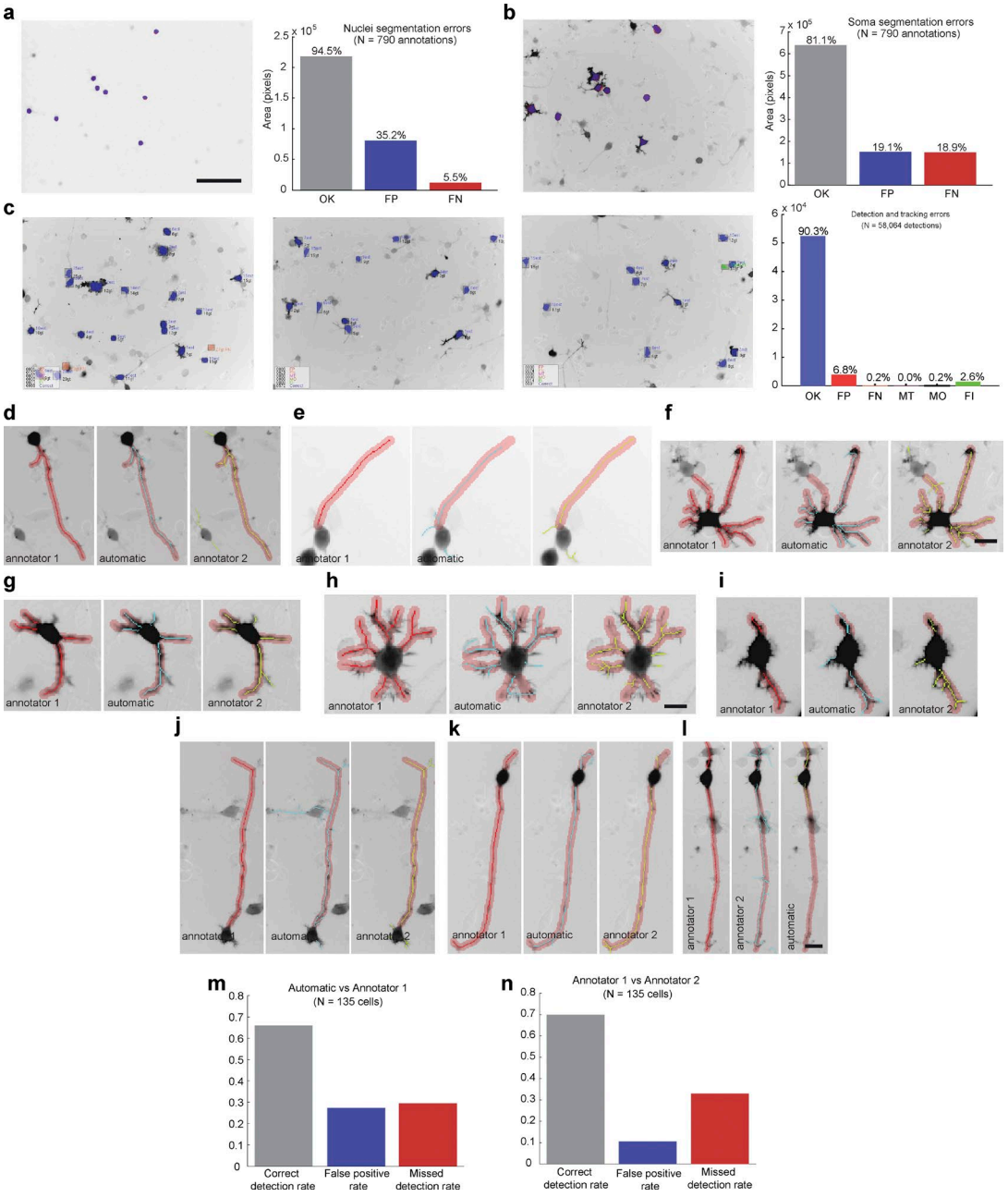

Figure S2. **Evaluation of the automatic soma and neurite segmentation and soma tracking.** (a) Nucleus segmentation evaluation. The ability of our method to segment nuclei was evaluated using a set of three hand-annotated movies from the screen. A total of 790 cells were annotated and then compared with the corresponding automatic segmentation. The annotation is shown as a red area in the left panel, and the automatic segmentation is depicted by the blue area. The overlap between the two areas is considered correct (the gray bar in the right panel). False positives occur in areas where the detection is present but without an annotation (blue bar in the right panel). False negatives occur where the annotation is not covered by a detection (red in the right panel). (b) Soma segmentation evaluation. The ability of our method to segment somata was evaluated using a set of three hand-annotated movies from the screen. A total of 790 cells were annotated and then compared with the corresponding automatic segmentation. The annotation is shown as a red area in the left panel, and the automatic segmentation is depicted by the blue area. The overlap between the two areas is considered correct (the gray bar in the right panel). False positives occur in areas where the detection is present but without an annotation (blue bar in right panel). False negatives occur where the annotation is not covered by a detection (red in the right panel). (c) Tracking validation. The ability of our method to detect and identify cells over time was evaluated using a set of 20 hand-annotated movies from the screen. A total of 58,064 detections were annotated (gray bounding box surrounding the soma) if the cell was tracked for more than five frames. Automatic detections are color-coded according to the evaluation result: blue indicates correctly detected; red, false positive; orange, false negative; brown, the tracker covered multiple annotations; magenta, the annotation was covered by multiple trackers; and green, an error occurred in maintaining the identity of the annotation. In the right panel, the results show that 90.3% of annotated cells were correctly tracked. Videos of the 20 evaluation sequences appear in Video 4. Bar, 100 µm (a–c). (d–l) Segmentations for nine example cells. Raw images are shown in inverted black/white contrast. In each panel, the first image shows the neurites annotated by expert 1 in red. The shaded region denotes the area where a matching annotation is considered valid (tolerance 4.5 pixels = 9 µm). In the second image, the annotations recovered using our automatic algorithm are shown in cyan. The third image shows the neurite annotation from a second expert. Bars: (d–f) 30 µm; (g–i) 20 µm; (j–l) 50 µm. (m) Bar graph demonstrating the ability of the algorithm to recover segmentations provided by annotator 1. (n) Bar graph showing the disagreement between annotator 1 and annotator 2 on the same set of cells. The level of disagreement between the two annotators is similar to that between the automatic method and annotator 1.

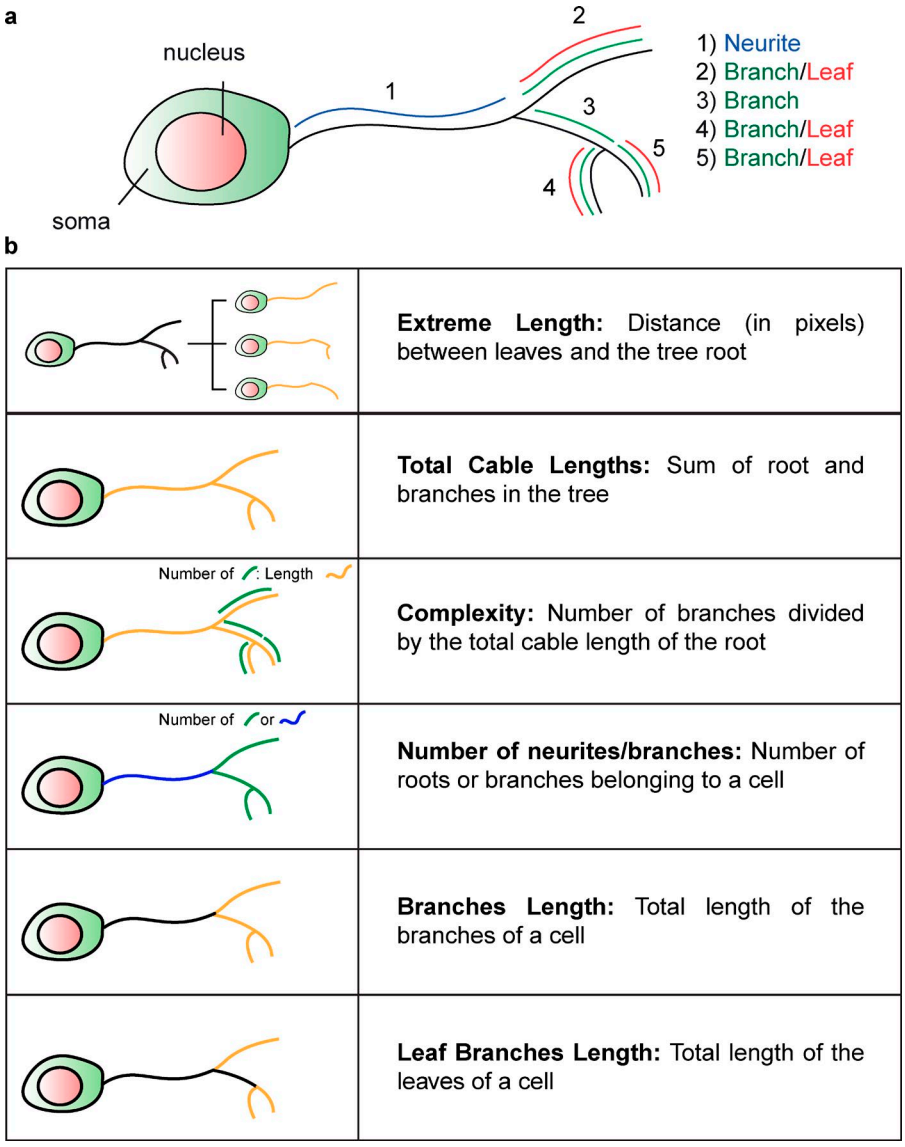

Figure S3. **Definition of parameters for feature extraction.** (a) Scheme representing different nucleus, soma and neurite components, as already shown in Fig. 2 b. (b) Explanatory schematics of different neurite-related parameters subsequently used to compute morphological and morphodynamic features.

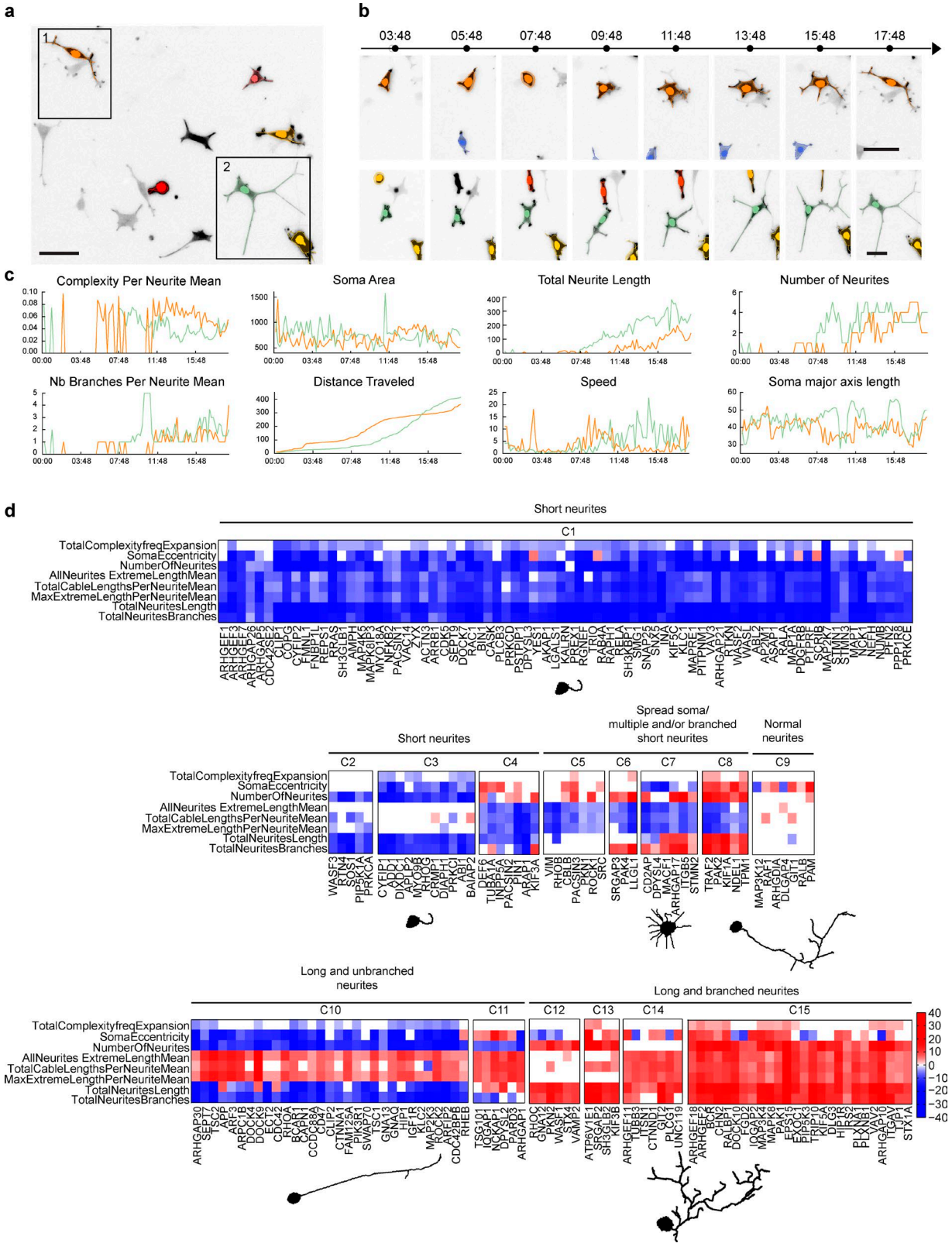

Figure S4. **PC-12 cell neuronal differentiation tracking and segmentation and hierarchical clustering of MDSs using the HS feature sets.** (a) Schematics of PC-12 Lifeact-GFP channel with superimposed nucleus, soma, and neurite segmentations color-coded according to cell identity. Bar, 100 µm. (b) Example of segmentation of two cells (from insets 1 and 2, shown in panel a). Nucleus, soma, and neurite segmentations are color-coded for cell identity. Time, h:min. Bar, 50 µm. (c) Temporal evolution of a set of features for the two cells shown in panel b. (d) Hierarchical clustering of MDSs using the HS feature set. Phenotypic clusters and representative images were extracted as described in Fig. 6.

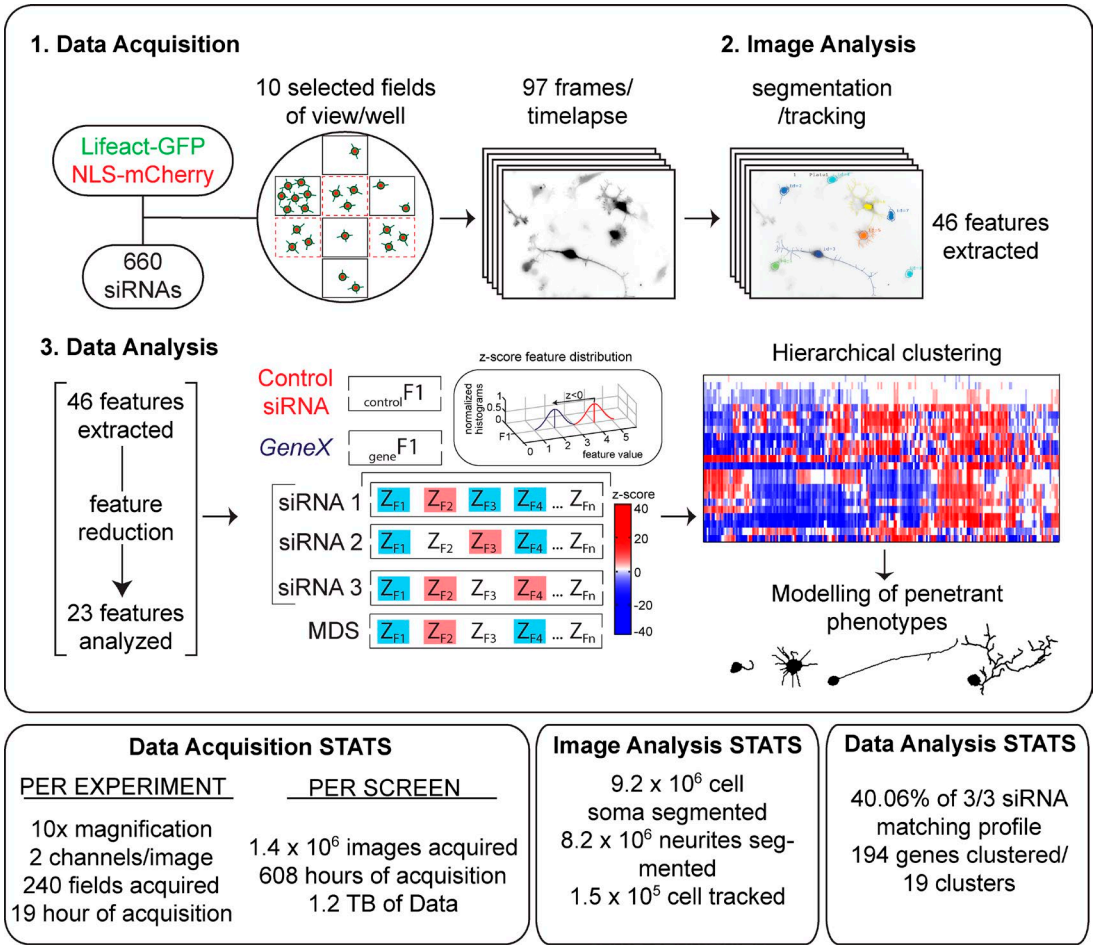

Figure S5. **Summary of workflow and statistics of the RNAi screen.**

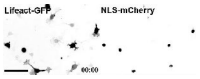

Video 1. **Raw movies of Lifeact-GFP/NLS-mCherry channels in N1E-115 cells.** Time-lapse video of N1E-115 cells cotransfected with control siRNA and Lifeact-GFP/NLS-mCherry is shown in inverted black-and-white contrast. Left: Lifeact-GFP channel; right: NLS-mCherry channel. Time scale is in h:min. Bar, 100 µm.

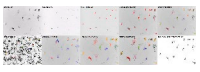

Video 2. **Dynamic visualization of different steps of the computer vision pipeline.** Different steps of the computer vision pipeline. From top left to bottom right: Lifeact-GFP channel, NLS-mCherry channel, detected nuclei marked in red, soma segmentation by region growing, cell identification over time using graph-based tracking, neurite-like structures detected using Hessian-based filter, calibrated likelihood of cell bodies, cell body segmentations after thresholding, backtracing neurite structures from candidate terminals, and final HDS-model graph representation. Bar, 100 µm.

Video 3. **Nuclei and somata segmentation evaluation.** The ability of our method to segment nuclei and somata was evaluated using a set of three hand-annotated movies from the screen. A total of 790 cells were annotated and then compared with the corresponding automatic segmentation. The annotation is shown as a red area, and the automatic segmentation is depicted by the blue area. Quantifications of correct detections, false positives, and false negatives are shown in Fig. S2.

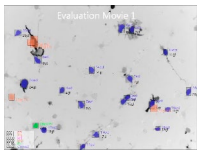

Video 4. **Soma detection and tracking validation.** The ability of our method to detect and identify cells over time was evaluated using a series of 20 hand-annotated movies from the screen. A total of 58,064 hand annotations appear as gray boxes surrounding the soma. Results of the automatic detection and tracking are color coded according to the result: blue, correctly detected; red, false positive; orange, false negative; brown, the tracker covered multiple annotations; magenta, the annotation was covered by multiple trackers; green, an error occurred in maintaining the identity of the annotation.

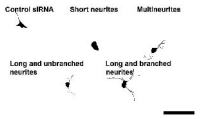

Video 5. **HDS-modeled graph representations of five global phenotypical classes.** HDS-modeled graph representations time-lapse video of the five phenotypical classes extracted from Fig. 6 is shown in inverted black-and-white contrast. From top left to bottom right: control siRNA, short neurite phenotype, spread soma/multiple and/or branched short neurites phenotype, long and unbranched neurite phenotype, and long and branched neurite phenotype. Bar, 100 µm.

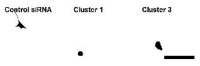

Video 6. **HDS-modeled graph representations of MDSs of dynamic short neurite phenotypes in the LS map.** HDS-modeled graph representations time-lapse video of the short neurite phenotypes extracted from Fig. 6 is shown in contrast. Left: control siRNA; middle: short neurite with low neurite dynamic phenotype (cluster 1); left: short neurite with normal neurite dynamic phenotype (cluster 3). Bar, 100 µm.

Video 7. **HDS-modeled graph representations of MDSs of dynamic long and branched neurite phenotypes in the LS map.** HDS-modeled graph representations time-lapse video of the dynamic long and branched neurite phenotypes extracted from Fig. 6 is shown in inverted black-and-white contrast. Left: control siRNA; middle: long and branched neurite with normal neurite dynamic phenotype (cluster 18); left: long and branched neurite with high neurite dynamic phenotype (cluster 19). Bar, 100 µm.

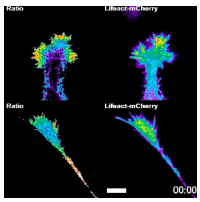

Video 8. **RhoA activation dynamics in advancing and collapsing growth cone in N1E-115 cells.** RhoA activation (ratio images) and Lifeact-mCherry (F-actin) were acquired by time-lapse epifluorescence microcopy using a Nikon Eclipse Ti microscope at one frame every 1 min. Movie plays at 5 fps. Bar, 10 µm. Time scale, min:s. Movie corresponds to Fig. 8 (a and b).

Video 9. **High-resolution time-lapse imaging of Dlc1 and p190RhoGAP KD growth cones in N1E-115 cells.** Lifeact-mCherry (F-actin) was acquired by time-lapse epifluorescence microcopy using a Nikon Eclipse Ti microscope at one frame every 5 s. Movie plays at 2 fps. Bar, 5 µm. Time scale, min:s.

Provided online is Table S1, which is a description of all siRNAs in the RNAi library.